Optical properties of liquid Se-Te alloys

Larry A. Silva and Melvin Cutler
Department of Physics, Oregon State University, Corvallis, Oregon 97331
(Received 30 May 1990)

Thin films have been used to determine the optical properties of the liquid-alloy system Se_xTe_{100-x} in the photon energy range of 0.4 to 5.0 eV, and at temperatures from the melting point to 500 °C. These liquids are semiconductors at Se-rich compositions, and undergo a transition to metallic behavior at high Te concentrations. The effects of this transition first appear in the optical data at 80 at. % Te. Possible forms for the electronic band structure in the semiconducting phase of the liquid are derived from the nondirect transition model for optical absorption. The optical properties of liquid Te (metallic phase) are separated into intraband and interband components, modeling the intraband component by Drude behavior, to test previously proposed mechanisms for the semiconductor-metal transition. Our results are consistent with the preservation of two-fold covalent bonding across this transition, and predict a ~0.4 eV gap between a Fermi level within the valence-band and the conduction-band edge. We have also measured the sub-band-gap absorption coefficient in semiconducting liquids containing 0, 20, and 40 at. % Te, and find that the extent of the exponential absorption edge decreases with increasing Te concentration.

I. INTRODUCTION

Much of the interest in the liquid alloy system Se_xTe_{100-x} stems from the observation that increasing the Te concentration, temperature, or pressure by a sufficient degree induces a transition in the electronic properties from those of a semiconductor to those of a poor metal.[1-3] This electronic transition is also accompanied by changes in the thermodynamic properties[4-6] and the local atomic coordination number in the liquid,[7-9] and the close correlation between these changes suggests that they are different aspects of the same transformation. At present, the nature of this common mechanism is not understood, and several models have been proposed to explain the experimental data. One model is based on the work of Cabane and Friedel.[10] They used the liquid Te neutron-diffraction data measured by Tourand and Breuil[11] as the basis of a model wherein the two-fold bonded chain molecules in the semiconducting Se-like structure are replaced by a metallic three-fold bonded structure similar to that in amorphous arsenic. Cutler, however, has noted that the bonding change proposed by Cabane and Friedel implies a *p-n* transition in the thermopower of the liquid, which, in fact, is not observed. The magnitude of the thermopower decreases, but remains positive across the semiconductor-metal transition. Cutler has suggested that the normal two-fold covalent bonding is maintained in the liquid, and the metallic properties are due to the introduction of a large density of hole states in the valence band as the number of broken bonds in the liquid becomes large.[12,13] In addition to models based on a homogeneous liquid structure, it has also been suggested that the metal-semiconductor transition may be due to the liquid being an inhomogeneous mixture of separate domains with semiconductor and metal-like properties.[14-16] In these models, the metal transition occurs as the relative concentrations of the two domains passes a percolative threshold for conduction.

The models outlined above imply significantly different changes in the electronic density of states. Clearly, direct information about the density of states in Se-Te liquids would be very useful in determining which may be correct. In the absence of techniques to perform photoemission spectroscopy on these liquids, the measurement of the optical dispersion properties provides the next best approach to probing the electronic structure. Fainchtein and Thompson,[17] and more recently Seyer *et al.*,[3] have used the energy dependence of the reflectivity of these liquids at normal incidence to determine their optical properties and to infer changes in the electronic structure. An analysis based solely on the reflectivity of the liquid has difficulties, however. It requires fitting functions with many independent parameters, and these parameters may not be well defined; and there is always the question of whether the optical properties of the surface are the same as those in the interior. An alternative approach to determining the optical dispersion is to measure both the reflectivity and transmissivity of a film of the liquid, which makes it possible to calculate the complex dielectric constant directly. This also provides a more direct probe of the electronic structure of the liquid volume (as opposed to the surface) through the determination of the absorption coefficient. In the past, experimental limitations on the minimum film thickness obtainable has precluded transmission measurements at photon energies where interband transitions take place. We have developed new techniques for preparing thin liquid films which have allowed us to produce Se-Te samples as thin as 0.2 μm, making it possible to measure the transmissivity well into the fundamental transition region.

In this paper we report data for the optical properties of Se-Te liquids covering the composition range from

pure Se to pure Te, and the photon energy range of 0.4 to 5.0 eV. In an effort to understand the electronic structure in the semiconducting phase of these alloys, we have examined their optical properties above the band gap using the nondirect transition model for optical absorption. We find that the simple parabolic band-edge model commonly applied to liquid semiconductors does not fit the data, and we discuss several possible ways of interpreting the optical behavior. We have also measured the absorption coefficient of the semiconducting liquids below the band gap. The exponential form of the absorption edge in Se is well known; our data show that this exponential behavior is gradually lost when Se is alloyed with Te. The most significant finding of this work concerns the semiconductor-metal transition. Evidence for the onset of this transition appears at the composition $Se_{20}Te_{80}$, and the data for liquid Te clearly show the presence of a large density of free carriers. We have separated the complex dielectric function of liquid Te into interband and intraband components, using the Drude model for the intraband part. Our results for the interband component are consistent with the preservation of two-fold bonding across the semiconductor-metal transition in the liquid.

II. EXPERIMENTAL DETAILS

Two methods were used to prepare the liquid films. In the first, an evaporated solid sample film and a surrounding evaporated gasket were sandwiched between two optical windows, and the sample was then melted to obtain the liquid. In the second, a drop of the liquid sample was pressed into a cavity between optical windows. A detailed account of these methods has been presented elsewhere.[18] In this section we will describe how the optical properties of the film samples were determined. The spectrometer used to measure the film reflectance and transmittance is shown in Fig. 1. An incident beam of chopped, monochromated light was partially reflected and transmitted by the cell. The magnitudes of the resulting detector signals were proportional to the reflectivity and transmissivity of the optical cell containing the liquid film. They were calibrated against a separate measurement of the reflectivity and transmissivity of an empty sample cell, using the known refractive index of fused quartz to determine the reflectance and transmittance of the filled cell ($R_{\text{cell}}, T_{\text{cell}}$). R_{cell}, T_{cell} were produced by the reflectance and transmittance of the liquid film ($R_{\text{film}}, T_{\text{film}}$), modified by the additional reflections at the window-air interfaces. The reflectivity of a quartz-air interface is small, about 4%, and the effect of the multiple reflections this produced within the optical cell was easily separated from R_{cell}, T_{cell} to obtain $R_{\text{film}}, T_{\text{film}}$.

The data for $R_{\text{film}}, T_{\text{film}}$ were related to the complex index of refraction of the liquid $n+ik$ through the general expressions[19]

$$T_{\text{film}} = tt^* = \left[\frac{(1-r^2)e^{-i(\delta - i\beta)}}{1-r^2 e^{-2i(\delta - i\beta)}} \right] \text{c.c.} , \tag{1a}$$

and

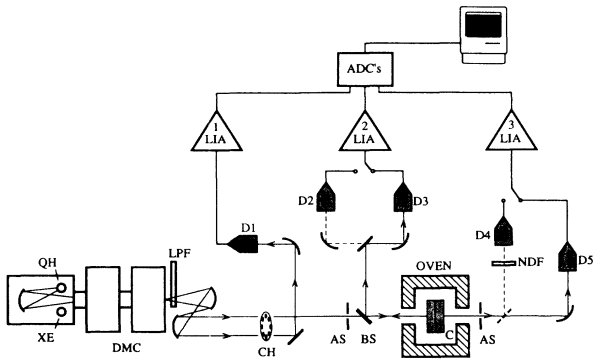

FIG. 1. Optical spectrometer: D1, pyroelectric detector; D2, PbS detector; D3, Si photodiode; D4, photomultiplier; D5, Si photodiode/PbS cell; QH, quartz-halogen lamp; XE, xenon arc lamp; LPF long-pass filter; DMC, double monochromator; LIA, lock-in amplifier; CH, chopper; AS, aperture stop; BS beam splitter; C, sample cell, NDF, neutral density filter.

$$R_{\text{film}} = rr^* = \left[-r + \left[\frac{r(1-r^2)e^{-2i(\delta - i\beta)}}{1-r^2 e^{-2i(\delta - i\beta)}} \right] \right] \text{c.c.} , \tag{1b}$$

where t and r are the transmittance and reflectance amplitudes of the film. The factors appearing in Eq. (1) are the Fresnel reflection coefficient $t = [n_0 - (n+ik)]/[n_0 + (n+ik)]$, the interference phase factor $\delta = (E/\hbar c)nd$, and the amplitude attenuation coefficient $\beta = (E/\hbar c)kd$, which in turn depend upon the refractive index of the windows n_0, the film thickness d, and the photon energy E. Equations (1a) and (1b) are multivalued, i.e., a given pair of values of the reflectance and transmittance measured at a single wavelength does not correspond to a unique set of values for n, k, and d. In this experiment it was necessary to determine the thickness of the film before calculating the index of refraction. For the thin-film samples ($d < 3.0$ μm) with an accessible region of transparency in the infrared, the thickness was determined from the interference fringes in the reflectivity data. This method provided the best values for d, with an accuracy of 1% for Se and $Se_{80}Te_{20}$, and 3% for the composition $Se_{60}Te_{40}$. The thicknesses of the thin-film alloys with no infrared transparency were determined indirectly, either from a surface profilometer scan of the film after it was frozen ($Se_{40}Te_{60}$ and $Se_{20}Te_{80}$), or by simply calculating it from the known mass and density of the sample, along with a measurement of the area of the film it formed between the windows (Te). The accuracy of the thickness found by these indirect methods is estimated to be 5%. For the thick films ($12\mu\text{m} < d < 25$ μm) used to measure the optical absorption below the band gap, d was determined by matching the calculated thick-film absorption coefficient with the thin-film results in the energy range where the two sets of data overlapped. Once a value for d was obtained, Eq. (1) was solved numerically to find the values of n and k at each energy which simultaneously produced the measured values for $R_{\text{film}}, T_{\text{film}}$.

There are two factors which limit the accuracy of the data: the alloy composition and the film thickness. Inaccuracies in the film thickness led to errors in k primarily through the product kd in the amplitude attenuation coefficient. This also affected the calculated value of n when k was large, since a shift in k requires an opposite shift in n to fit the measured reflectivity. The mass measurements used to control the alloy compositions were very precise (four significant digits). Still, the optical data exhibited systematic energy shifts between identically prepared samples, which were interpreted to arise from variations in the composition in the range of $\pm 3\%$; e.g. the composition of a nominal $Se_{60}Te_{40}$ alloy fell between $Se_{63}Te_{37}$ and $Se_{57}Te_{43}$. This shift may have been due to differences in the composition of the initial ~ 0.3 mg solid alloy used to make the film in the case of the compressed-liquid films. The same master set of alloy materials was used throughout the experiment, so this would require fluctuations in x within the volume of the master alloys. In the case of the samples formed by evaporation, the variations in composition were attributed to a small leakage of the liquid into the gasket region when the solid films were melted. The Se and Te film layers melted unevenly and at different temperatures, and an excess of one component of the liquid would result if more of the other component leaked past the gasket. The results to be given here are the average of all the measurements made at each composition.

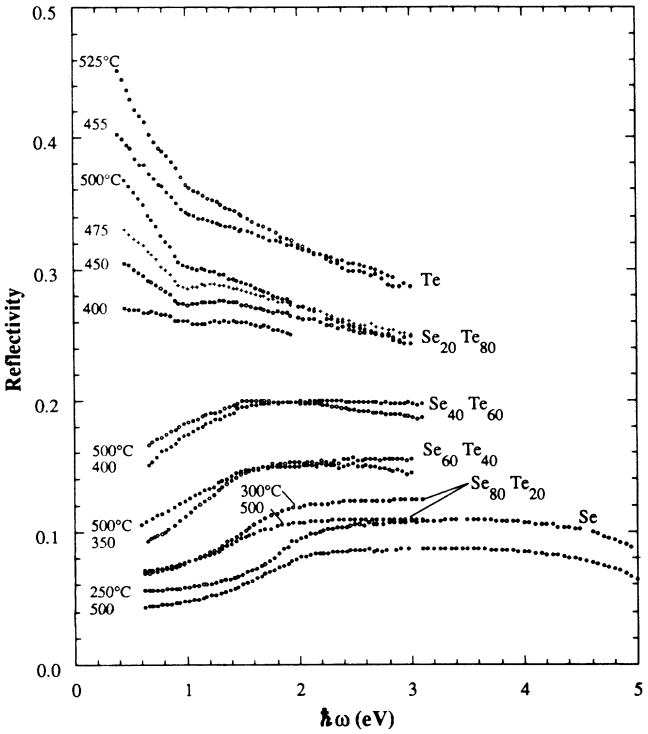

FIG. 2. Reflectivity of liquid Se-Te alloys behind a quartz window.

III. RESULTS

Figure 2 shows a representative set of curves for the reflectivity of a fused quartz–liquid Se_xTe_{100-x} interface as a function of composition and moderate temperature changes. Several of the characteristics of the Se-Te system can be seen by examining the reflectivity data by itself. Starting with pure selenium, R is fairly flat in the infrared up to about 1.5 eV, and then it rises to a higher plateau above 2 eV. This change is characteristic of a semiconductor with a large energy gap—in this case ~ 2 eV. As the Te concentration is increased the reflectivity rises and the band gap decreases. The red shift of the band gap can be seen in the alloys containing 20–60% Te by the shift in the rising edge of the reflectivity curve to lower energies. There is a noticeable change in the optical behavior between 60% Te and 80% Te, however. Below 1 eV the reflectivity of liquid Te, and liquid $Se_{20}Te_{80}$ at higher temperatures, increases at lower energies, as expected when a large number of free charge carriers are present. This is the result of the semiconductor-metal transition in the liquid. A clearer picture of this transition is seen in the data for the optical absorption α, shown in Fig. 3. The most striking feature in these data is the linear behavior of α, which in the case of liquid Se extends nearly 1.5 eV above the band gap. As in the case of the reflectivity, the alloy $Se_{20}Te_{80}$ is a pivotal composition. The absorption begins to increase more rapidly at lower photon energies, which lowers the slope, and the temperature dependence of α becomes large. At low temperatures, liquid $Se_{20}Te_{80}$ still appears to be a semiconductor in that extrapolating the absorption curves to zero α still gives a positive energy gap. Liquid Te, however, has a negative extrapolated energy gap.

A complete description of the optical properties of Se-Te liquids is given by the complex dielectric function $\epsilon = \epsilon_1 + i\epsilon_2$ shown in Figs. 4–7. The complex dielectric function of liquid Te has been plotted on a separate graph for clarity (Fig. 7). With the exception of the 500 °C data, the ϵ_1 data for Te are scattered about a common curve and do not display a consistent temperature dependence. The large scatter in ϵ_1 is caused by the large value of k, which makes it sensitive to small errors in the reflectivity. As an example, the 500 °C results can be brought in line with the others with a 3% increase in R, which is within the experimental uncertainty. The imaginary part of the dielectric function ϵ_2 is much less sensitive to inaccuracies in the reflectivity. This is because it depends on the product of n and k, and their errors tend to cancel when taking the product.

Data for the absorption edges below the band gap of Se, $Se_{80}Te_{20}$, and $Se_{60}Te_{40}$ are shown in a semilogarithm plot in Fig. 8. The absorption coefficient of liquid selenium increases exponentially with photon energy below 5000 cm^{-1}. This exponential form for α has also been observed in amorphous and crystalline Se, and is an example of a general phenomena seen in a wide variety of materials, known as Urbach absorption.[20] The alloys containing 20% and 40% Te differ from Se in that α rises above the exponential form at the low-absorption end of the data. The properties of the absorption edge will be discussed further in Sec. IV.

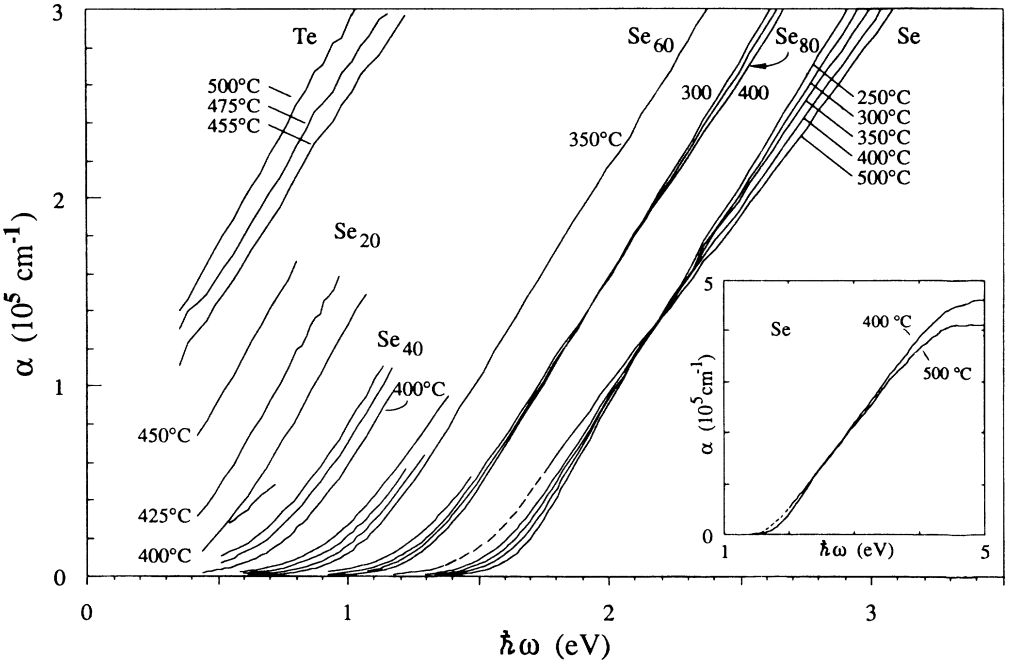

FIG. 3. Absorption coefficient of liquid Se_xTe_{100-x} alloys. Alloy compositions are indicated in at. % Se.

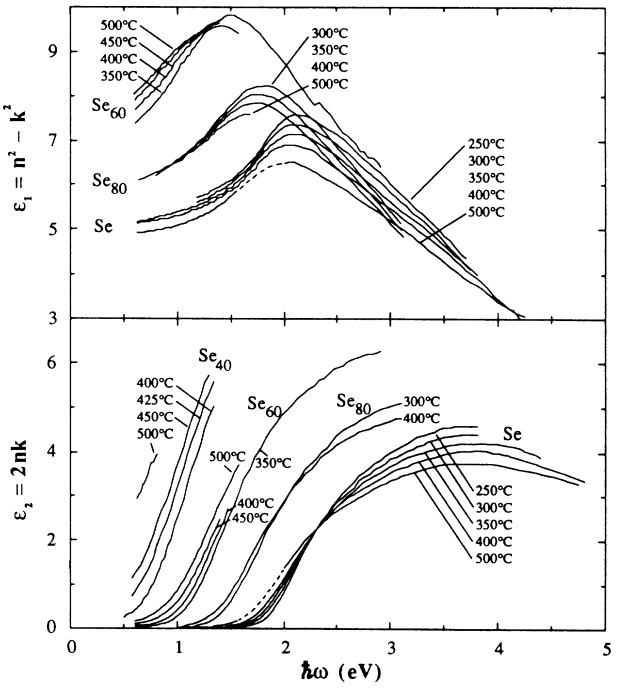

FIG. 4. Real ϵ_1 and imaginary ϵ_2 parts of the dielectric constant of Se-rich, Se-Te liquids. The alloy compositions are indicated in at. % Se.

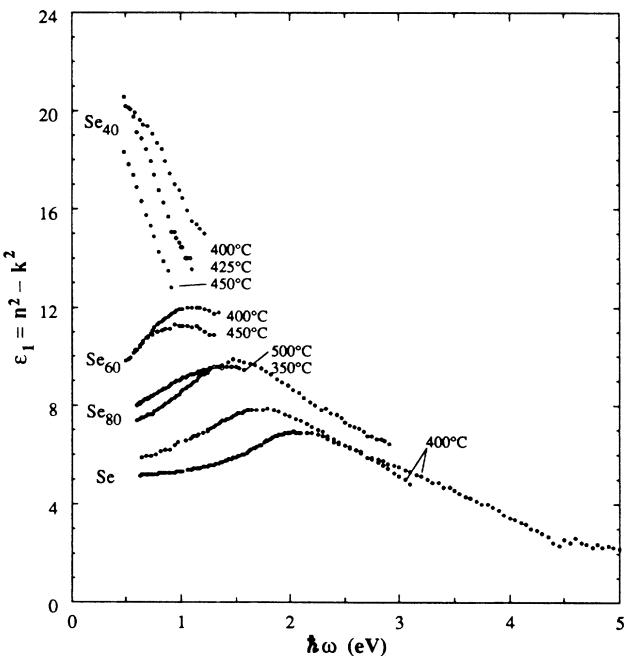

FIG. 5. Real part of the dielectric constant of Se-Te liquids, showing the behavior of the Te-rich liquids against a representative set of curves for the Se-rich liquids. Alloy compositions are indicated in at. % Se.

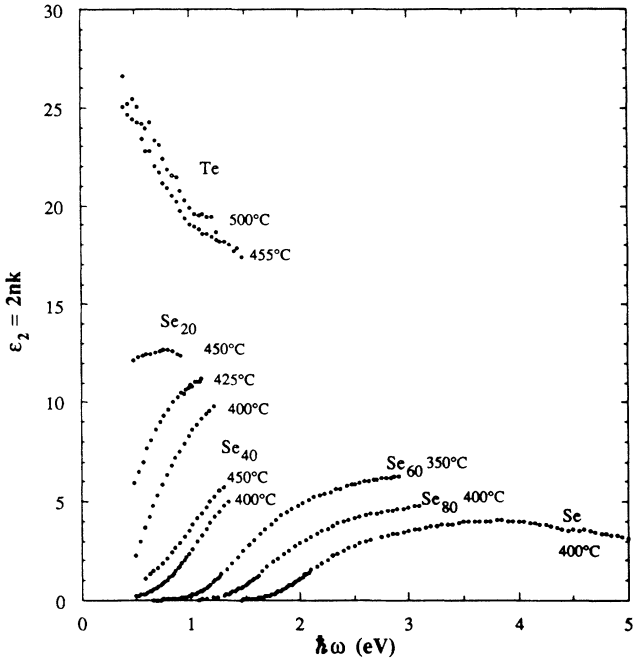

FIG. 6. Imaginary part of the dielectric constant of Se-Te liquids, showing the behavior of the Te-rich liquids against a representative set of curves for the Se-rich liquids. Alloy compositions are indicated in at. % Se.

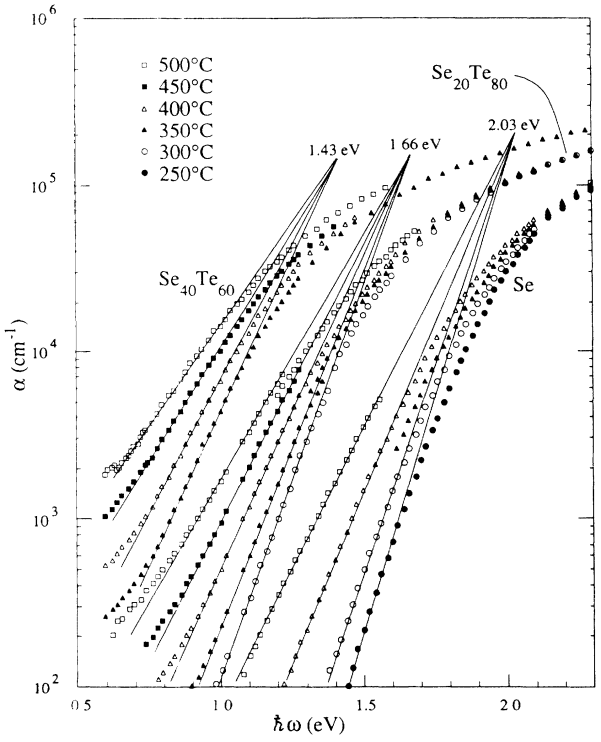

FIG. 8. The absorption edges of liquid Se and alloys containing 20 and 40 at. % Te. The steepness coefficients found in fits to the spectral Urbach rule are Se ($0.717-2.64\times10^{-4}$ T), $Se_{80}Te_{20}$ ($0.778-4.28\times10^{-4}$ T), and $Se_{60}Te_{40}$ ($0.795-5.60\times10^{-4}$ T), where T is measured in K.

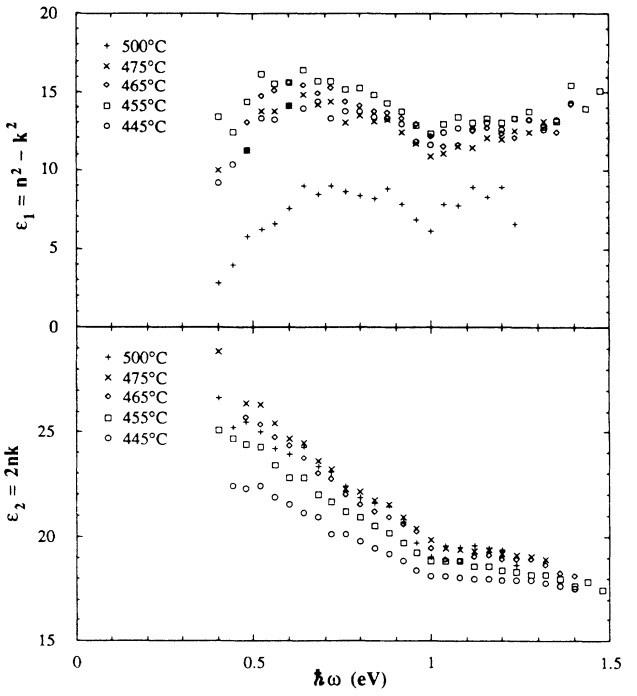

FIG. 7. Real ϵ_1 and imaginary ϵ_2 parts of the dielectric constant of liquid Te.

IV. ANALYSIS OF THE OPTICAL DATA

A. The density of states in the semiconducting alloys

The primary effect of alloying Se with increasing amounts of Te is to decrease the gap between the conduction and valence bands in the liquid. We have somewhat arbitrarily chosen to define the optical band gap E_g as the energy at which an extrapolation of the linear portion of the absorption curve crosses the zero α axis. The corresponding values for E_g are plotted as a function of temperature in Fig. 9. At temperatures near the melting point, the gap energy decreases from a value of 1.84 eV for Se to 0.53 eV for $Se_{20}Te_{80}$. This behavior can be understood qualitatively by noting that the two-fold bonded chain structure in trigonal Se and Te crystals is still present in the semiconducting liquid phase. Trigonal Se has a band gap of 2.0 eV, and the band gap in trigonal Te is 0.32 eV; the steady decrease in the band gap of the alloys reflects the electronic differences in the covalent bonds formed by Se and Te atoms in the long-chain structure.

The optical data show directly how the gap between the conduction and valence edges changes with temperature and composition. It is also of interest to see if this data can give information about the form of density of states at different temperatures and compositions. Tauc has related the band structure of disordered materials to

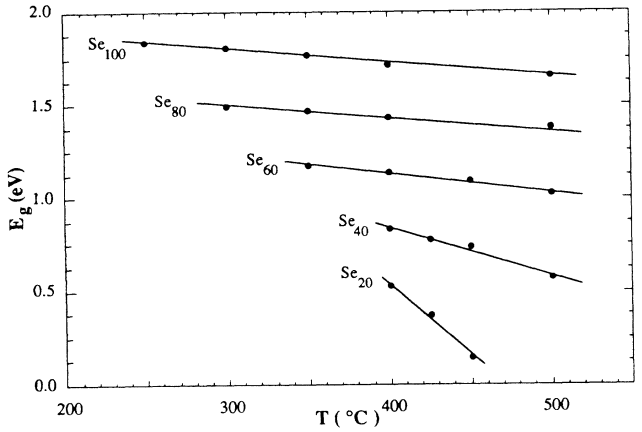

FIG. 9. The optical band gap of Se-Te liquids as a function of temperature. Alloy compositions are indicated in at. % Se.

their optical properties by assuming that the wave-vector conservation rule is totally relaxed in any photon-induced electronic transition.[21] In this "nondirect transition model" (or NDT model) the imaginary part of the dielectric function is given by

$$\epsilon_2 = 2\Omega \left[\frac{\pi e}{m\omega}\right]^2 \int_{-\infty}^{\infty} N_v(E) N_c(E+\hbar\omega) |M(\hbar\omega)|^2 dE \ , \tag{2}$$

where $N_c(E)$ and $N_v(E)$ are the conduction- and valence-band densities of states, respectively, and $|M|^2$ is the average squared dipole matrix element between all states which can be coupled by a photon of energy $\hbar\omega$. The NDT model accounts for the optical properties of many disordered materials in a simple way if it is also assumed that the energy dependence of the band edges can be represented by power-law functions separated by a band gap E_g, i.e., $N_c \propto (E-E_g)^{r_c}$ and $N_v \propto E^{r_v}$, and that $|M|^2$ is independent of photon energy. Justification for the constant dipole matrix approximation is often given in terms of Hindley's random phase model for amorphous semiconductors.[22] These two approximations allow the integration in Eq. (2) to be performed, yielding $\epsilon_2 \propto (\hbar\omega)^{-2}(\hbar\omega - E_g)^r$, where $r = r_c + r_v + 1$. The energy dependence of ϵ_2 for many disordered materials is consistent with $r=2$. This agrees with the usual view that both band edges should be close to parabolic, and therefore $r_c = r_v = \frac{1}{2}$. A similar analysis of the optical data for the semiconducting Se-Te liquids, however, has shown that this simple explanation does not apply. The ϵ_2 data for the alloys containing 0–40% Te are fitted with r in the range of 1.0 to 1.1 over an energy interval of ~ 1.5 eV above the band gap. This is significantly different from the value of 2 predicted for parabolic band edges, and suggests that there is something unique about the electronic structure in these liquids. We have used the NDT model to deduce possible forms for the band structure by making three different simplifying assumptions about the energy dependence of the unknown functions in this model—N_c, N_v, and $|M|^2$. A summary of this work is given below.

(i) A comparison of the measured band structure of crystalline and amorphous Se and Te with the calculated structure[23] suggests that the band edges may be fairly symmetric in the liquid. If both band edges have the same energy dependence, and $|M|^2$ is assumed to be constant, then Eq. (2) reduces to $\epsilon_2 \propto (\hbar\omega)^{-2} \int N(E) N(E-\hbar\omega) dE$. Curves for $N(E)$ which match the measured ϵ_2 data have been calculated using an iterative numerical integration procedure. The results are shown in Fig. 10. These curves are for the position and shape of conduction band, with the valence band being the mirror image starting at the origin of the energy

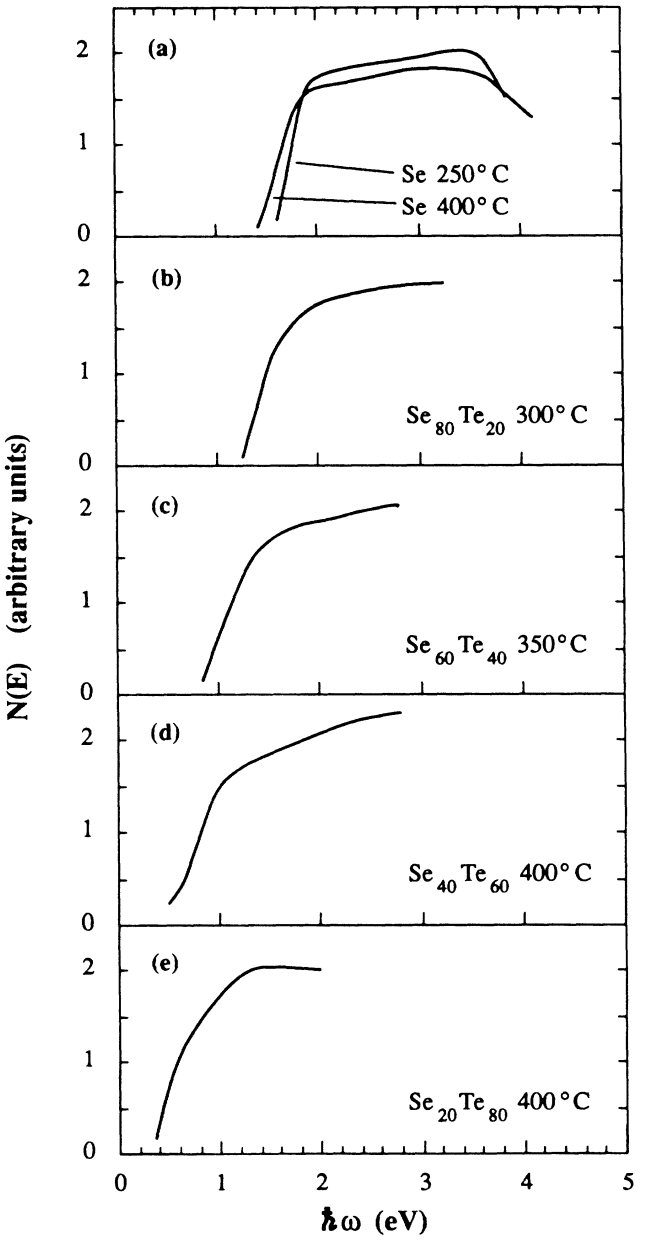

FIG. 10. Band edges in the semiconducting liquids, calculated under the assumptions $N_v \approx N_c$ and $|M|^2$ constant. The curves shown are for the conduction band; the valence band is the mirror image extending below the origin.

axis. If the assumption $N_c \propto N_v$ is correct, the band edges of Se at 250 °C are fairly steep, followed by a slow rise in the density of states up to 3.5 eV. Increasing the temperature or Te concentration broadens the edge, and it appears that at low temperatures the band edges in $Se_{20}Te_{80}$ are nearly parabolic.

(ii) A second possibility is to assume that the valence band is parabolic at all compositions, as it was found by Kao and Cutler to be in Te-rich liquids.[1] [They also observed a linear dependence closer to the band edge, but that may be attributed to band tailing due to local electrostatic potential fluctuations, which would not show up in the integration leading to Eq. (2).] Taking $|M|^2$ to be constant again, the curves calculated for $N_c(E)$ are shown in Fig. 11. The shape of the band edge in Fig. 11(a) is similar to the density of states expected in a one-dimensional conductor, which suggests that the electron states in the conduction band may have one-dimensional characteristics. This, in turn, implies very dissimilar electron wave functions in the conduction and valence bands, since a parabolic valence band comes from three-dimensional electronic states. The long-chain structure of liquid Se does lend itself to the possibility of states with both one- and three-dimensional character. The valence band is composed of lone-pair p orbitals which form weak bonds between chains, while the conduction band is formed by antibonding orbitals with a higher probability density within a chain, and therefore may be more "one-dimensional."

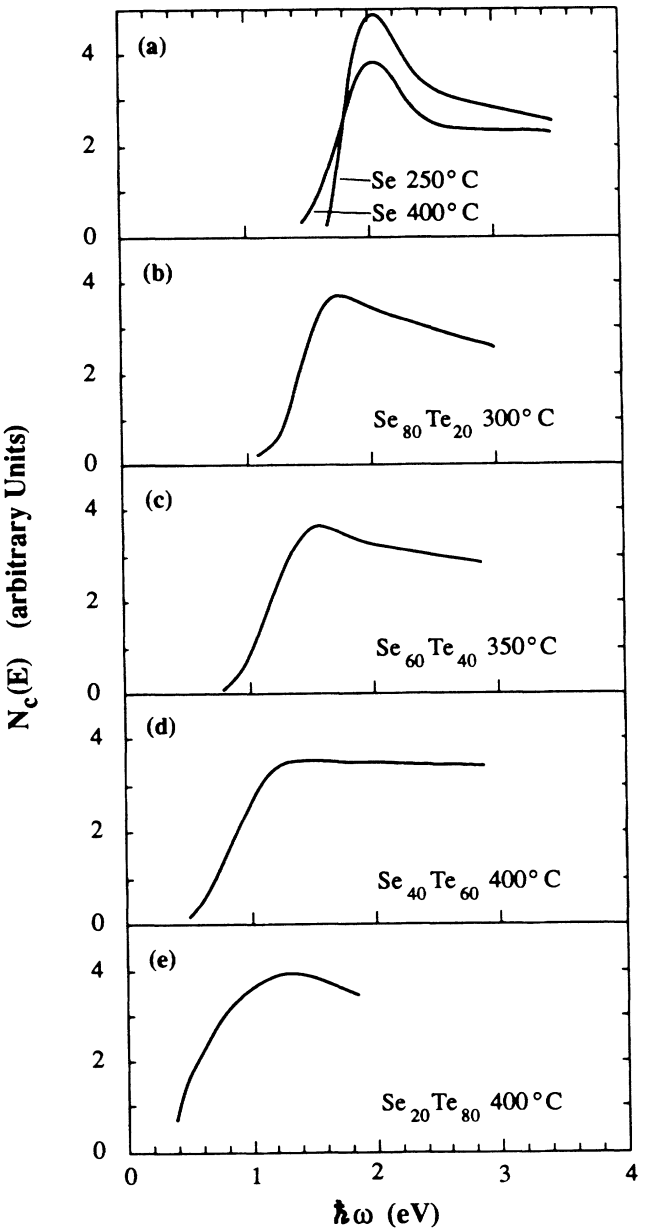

FIG. 11. Conduction band in the semiconducting liquids, assuming the valence band is parabolic and $|M|^2$ is constant.

(iii) Considering the prevalence of parabolic band edges among disordered semiconductors, it is conceivable that Se-Te alloys also have parabolic conduction- and valence-band edges, and the apparent discrepancy in the measured form of ϵ_2 is due to the energy dependence of the dipole matrix function. The integral in the NDT model cannot be directly evaluated without knowing the form of $|M|^2$, but following Maschke and Thomas [24] we can define a new function $|\bar{M}|^2$ which represents the *averaged* effect of the dipole matrix function on the convolution of the density of states. This new matrix function gives a relative measure of the effect of the dipole matrix elements on the optical properties of the liquid. For a material with parabolic band edges, $(\hbar\omega - E_g)^2|\bar{M}|^2 \propto (\hbar\omega)^2\epsilon_2$. Curves for $|\bar{M}|^2$ calculated from ϵ_2 and the optical gap data in Fig. 9 are given in Fig. 12. It is noteworthy that the results for liquid Se look similar to those found by Maschke and Thomas for amorphous Se. Their same interpretation may, therefore, also apply to liquid Se at the melting point, i.e., the structure of the liquid is similar to that of trigonal Se, and therefore the energy dependence of the matrix elements should be about the same with the details originating from long-range order removed. The effect of increasing the temperature or Te concentration in the liquid is then to increase the disorder, which reduces the energy dependence

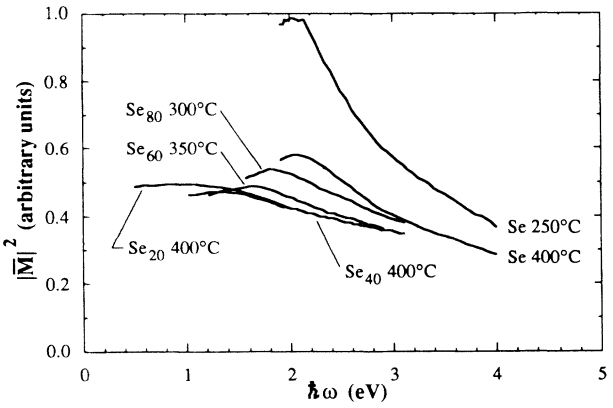

FIG. 12. The energy dependence of the average dipole function $|\bar{M}|^2$. These curves are based on parabolic densities of states in the conduction and valence bands.

of the matrix element function. One implication of this view is that the random-phase model proposed by Hindley does not apply to Se, because the energy dependence of $|\overline{M}|^2$ is considerable.

The three band-structure models discussed above represent three extremes of simplification, and the actual situation may well lie between them. At the Se-rich end of the composition the bands predicted by these models are quite different, but it appears that at the composition $Se_{20}Te_{80}$ they all converge to the simple case of two parabolic bands with a constant dipole matrix.

B. The absorption edge

There are two features in the absorption-edge data: approximately exponential behavior below ~ 5000 cm^{-1}, and in the case of the alloys, a nonexponential tail at the lowest measured values of α. The exponential feature is very common among liquid and amorphous semiconductors. Generally such data are quantified in terms of the spectral Urbach rule[20]

$$\alpha = \alpha_0 e^{(\hbar\omega - E_0)\sigma/kT}, \tag{3}$$

where the parameters E_0, σ, and α_0 are material dependent, and may be temperature dependent as well. We have fitted the exponential region of the data in Fig. 8 to Eq. (3), though the results for $Se_{80}Te_{20}$ and $Se_{60}Te_{40}$ are of limited value because of the poor definition of the exponential range. The steepness factor σ decreases linearly with T over the temperatures measured. Expressions for the temperature dependence are given below Fig. 8. The "focal-point" energies E_0 are also indicated in the figure, and the prefactor α_0 has the constant value $e^{12.0\pm0.2}$. Our σ data for Se are larger (steeper slopes) than those previously reported.[25–27] The absorption edge of Se-Te alloys has also been measured by Perron.[27] His $Se_{80}Te_{20}$ results for σ are much lower than those given here, but they were based on absorption coefficient measurements below 10^{-3} cm^{-1}, which the data in Fig. 8 indicate, is not entirely exponential.

The deviations from the Urbach rule in the alloy samples are large in comparison with other liquid semiconductors. For example, liquid S, AsSe, As_2Se, and $Ge_{10}Se_{90}$ all show exponential absorption down to 10 cm^{-1} before tailing in the edge appears. The reason for the large absorption tail is not known. One possible way to explain the increase in α at low energies is to assume that there are local fluctuations in the dielectric constant in the liquid, which could lead to a significant amount of scattering of the incident light at low absorption levels. Fluctuations in the dielectric function would result, for example, if Te atoms bonded together more often than with other Se atoms in the melt. Optical scattering of this type has been observed in liquid sulfur at temperatures near the polymerization transition,[28] though at absorption levels much lower than seen in Fig. 8. There is no evidence of concentration inhomogeneities in the optical data above the band gap, however. This point will be returned to after the metal-semiconductor transition is examined in the next section.

C. Metal semiconductor transition

In comparison with the other manifestations of the metal transition (e.g., conductivity and compressibility changes), the optical behavior indicates a semiconductor-metal transition at a composition considerably richer in Te, between 80 and 100 at. % Te. Considering the three types of models for the metal transition discussed in the Introduction, the optical data seem to be most consistent with the model proposed by Cutler. The electronic structure for this model is shown in Fig. 13. In the metallic phase, there is a large number of vacant states at the top of the valence band, created by the absorption of a partially filled acceptor band due to broken bonds into the valence band. The conduction-band edge lies above the Fermi energy and thus makes no contribution to the dc conductivity. With the Fermi energy below the conduction-band edge, the optical absorption can be decomposed into two parts, one due to interband transitions of the same nature as in the semiconductor, and a second part due to intraband transitions in the valence band. We will show that our data are consistent with this analysis, and we are able to deduce a positive gap between the Fermi energy and the bottom of the conduction band.

The intraband contribution to the optical behavior can be estimated using the Drude model for free-carrier absorption. Expressed in terms of the complex conductivity $\sigma_1 + i\sigma_2$, the optical properties of a Drude metal are given by[29]

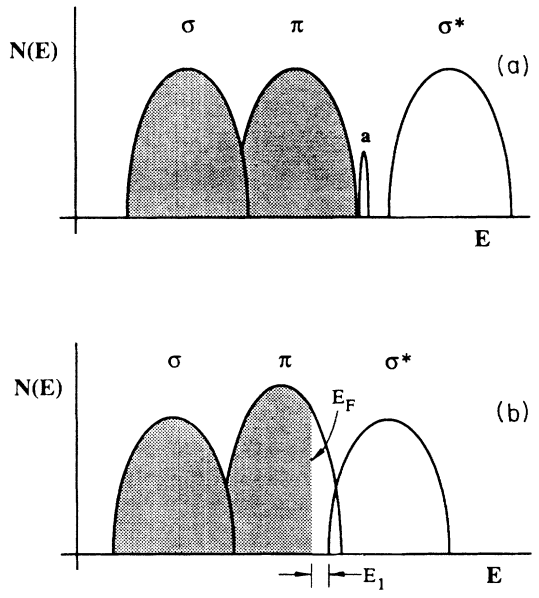

FIG. 13. Semiconductor-metal transition in Se-Te liquids as proposed by Cutler. (a) σ and σ^* bands are from intrachain bonding; lone-pair p orbitals from the π band. Broken bonds produce acceptor states a, and as the density of these defects increases an acceptor band shifts into the valence band (b). The Fermi level E_f falls at an energy E_1 below the conduction-band edge.

$$\frac{\sigma_1}{\omega}=\frac{\sigma_0\hbar}{(\hbar\omega)+(\hbar\omega)^3(\sigma_0 m^*/\hbar n e^2)^2}\ ,$$
$$\frac{\sigma_2}{\omega}=\frac{(\sigma_0 m^*/ne^2)}{1+(\hbar\omega)^2(\sigma_0 m^*/\hbar n e^2)^2}\ . \tag{4}$$

The three parameters appearing in Eq. (4) are the electron effective mass m^*, the dc conductivity σ_0, and the density of charge carriers per unit volume n. Of the three, the dc conductivity of the liquid is the most accurately known. Perron's data for σ_0 at 445, 475, and 500 °C are listed in Table I. The optical effective mass m^* is expected to be larger than the free-electron mass m_e, but its value can only be estimated. Kao and Cutler have determined an effective electron mass for the transport properties of Te-rich Se-Te liquid alloys. They obtained values of $2.45m_e$ for $Se_{20}Te_{80}$ and $2.38m_e$ for $Se_{10}Te_{90}$. We have taken the optical effective mass in liquid Te to be $2.38m_e$, with an uncertainty of perhaps $\pm 0.5m_e$. The hole density in the liquid was determined in two ways. First it was assumed that the valence band is basically parabolic in form, as suggested by the band-structure calculations for $Se_{20}Te_{80}$ in Sec. IV A. If follows that n is related to the density of states at Fermi energy $N(E_F)$ and the effective mass by

$$n=\frac{h^6\pi^4}{3m^{*3}}N^3(E_F)\ . \tag{5}$$

The density of states at the Fermi energy was found from the magnetic susceptibility of the liquid, which is given by

$$\chi_m=\chi_d+(\alpha-\beta)\mu_B N(E_F)\ . \tag{6}$$

Here χ_d is the diamagnetic contribution of the atomic cores, and the remaining term is the sum of the Pauli paramagnetic and Landau diamagnetic properties of the holes. Following Gardner and Cutler,[2] we made the approximation $(\alpha-\beta)=1$, and used the magnetic susceptibility of Te at room temperature for the core diamagnetism. The results for the hole densities are listed in the table under column n_1. The second method to determine n was based on the empirical curve found by Cutler *et al.* relating the hole density in Te-rich liquids to the volume contraction in the liquid.[30] Interpolating along this curve at points corresponding to the volume contraction of liquid Te, the values for the hole density listed under column n_2 were obtained. In view of the approximations involved, the agreement between n_1 and n_2 is considered good. We have arbitrarily chosen to use n_2 for the hole densities in the optical intraband calculations.

TABLE I. The free-carrier parameters for the valence-band holes.

T(°C)	σ_0(10^3 Ω^{-1} cm^{-1})	$m^*(m_e)$	n_1 (10^{22} cm^{-3})	n_2 (10^{22} cm^{-3})
445	1.70	2.38	1.49	1.21
475	1.91	2.38	1.76	1.48
500	2.07	2.38	2.01	1.66

The measured dielectric function $\epsilon_{1m}+i\epsilon_{2m}$ of liquid Te was separated into interband $\epsilon_1+i\epsilon_2$ and intraband $\sigma_1/\omega+i\sigma_2/\omega$ components through Eq. (4) and the general relations

$$\epsilon_{1m}=\epsilon_1-\frac{\sigma_2}{\omega}\ ,$$
$$\epsilon_{2m}=\epsilon_2+\frac{\sigma_1}{\omega}\ . \tag{7}$$

The results for Te at 445 °C, shown in Fig. 14, indicate the relative magnitudes of these factors. The curve for ϵ_2 clearly shows the energy dependence expected for a gap between the Fermi level and the conduction-band edge (compare the behavior of ϵ_2 in the semiconducting liquids). The data for the interband dielectric function were used to determine the absorption coefficient the liquid would have if the intraband processes were "turned off." This is plotted in Fig. 15 for Te at 445, 475, and 500 °C. The points fall roughly along the same curve, and the intercept with the energy axis, corresponding to the energy E_1 in Fig. 13, is approximately 0.4 eV. The sensitivity of these results to the parameters used in the Drude model was checked by changing the ratio m^*/n appearing in Eq. (4) by a factor of 2 and 0.5. This had the effect of moving E_1 to 0.2 and 0.5 eV, respectively, but the gap between the Fermi energy and the conduction-band edge remained.

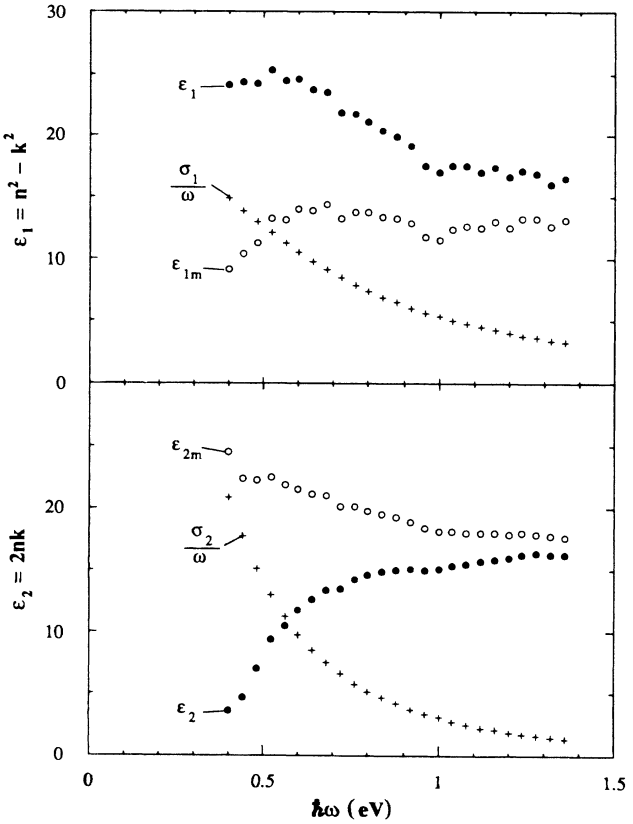

FIG. 14. The measured complex dielectric constant of liquid Te at 445° C, $\epsilon_{1m}+i\epsilon_{2m}$, separated into interband $\epsilon_1+i\epsilon_2$ and intraband $(\sigma_1+i\sigma_2)/\omega$ components.

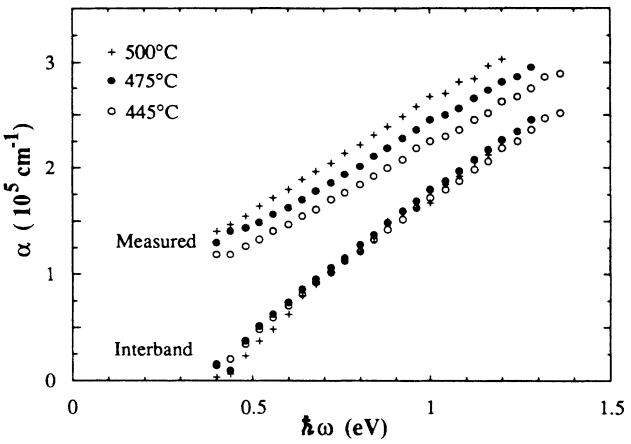

FIG. 15. Data for the measured absorption coefficient of liquid Te plotted with the calculated interband contribution.

V. SUMMARY AND DISCUSSION

The fundamental absorption-edge data for semiconducting Se-Te liquids shifts down in energy with increasing Te concentration in the manner expected if the Te atoms randomly replace Se atoms in chains of two-fold covalently bonded atoms. We have deduced three possible forms for the band structure from this data: steep, symmeteric band edges, a parabolic valence band with an effectively one-dimensional conduction band, and parabolic band edges with a photon-energy-dependent dipole matrix function. These band structures are based on different simplifying assumptions within the nondirect transition model for optical absorption, and can only be considered as guides for future work in understanding the electronic structure of these liquids. The onset of the transition to the metallic phase appears in the optical data at the composition $Se_{20}Te_{80}$ at high temperatures. This transition produces a gradual loss of the semiconductor band gap, but no other marked change in the absorption. This is consistent with Cutler's metallic transition model, which predicts that the transition procedes via the gradual shift of a partially filled acceptor band into the valence band. We have shown that the optical properties of Te also agrees with this process. Using the Drude model to estimate the optical properties of the valence holes, we were able to infer the presence of a 0.4 eV gap between the Fermi level and the bottom of the conduction band.

The other metal-transition models mentioned in the Introduction are not easily reconciled with the optical data. If the liquid structure is heterogeneous, then it would seem appropriate to model the changes in the optical behavior with the effective medium theories developed for composite materials, but we were unable to correlate the dielectric properties of the liquid in the semiconducting and metallic states with this approach. The model of Cabane and Friedel, on the other hand, differs from Cutler's model in having the valence band of the nonbonding electrons replaced by the lower-lying σ bonding band, and the metallic behavior is caused by the overlap of the conduction band with this lower band. This corresponds to the Fermi energy being above the conduction-band edge in Fig. 13, with the bottom band now being the σ bonding band. This electronic structure would also give rise to two contributions, interband and intraband, to the optical absorption, with the interband part now corresponding to the electrons in the conduction band. As in the case of the dc transport, however, it does not seem possible to make a continuous connection between the semiconductor and the metallic compositions for the size of the gap derived from the interband part of the optical absorption.

The apparent persistence of twofold covalent bonding across the semiconductor-semimetal transition has interesting consequences for the microscopic structure of the metallic liquids. The high concentration of holes in Te requires a high concentration of broken bonds, and therefore very short chains. The hole densities in Table I correspond to an average chain length of 4.0 atoms at 445 °C, and 3.3 atoms at 500 °C. The electronic transition is consistent with this shift to small molecular units, but there remains the question as to what causes the thermodynamic transition in the liquid. A decrease in the compressibility and increase in the density are also associated with the semiconductor-metal transition; these changes call for the introduction of a new type of bonding interaction between the atoms. Undoubtably, this new interaction must somehow be related to the short length of the two-fold bonded units in the liquid. Another clue to this puzzle is found in the x-ray and neutron-diffraction studies of the local structure in liquid Te. Dating back to the early diffraction measurements of Breuil and Tourand, there has been a tendency to interpret tellurium's radial distribution data in terms of a transition to three-fold coordination. But a recent reexamination of the data by Enderby and co-workers has led them to conclude that there is substantial penetration of the first coordination sphere by *noncovalently* bonded atoms.[31] The implication of this view is that there is a nondirectional bonding interaction in the liquid between neighboring twofold bonded molecules which allows atoms on these molecules to approach one another at distances near the covalent bond distance, but without appreciably altering the covalent band structure. Recently Cutler *et al.*[30] have proposed that this secondary bonding interaction could be attributed to electrostriction: a negative ion at the end of one covalently bonded molecule may polarize a neutral atom on a neighboring molecule, thus causing an electrostatic bonding interaction. The effects of electrostriction were calculated using macroscopic concepts and parameters in a domain which should properly be treated microscopically, and their numerical results are therefore of limited accuracy. The results do show, however, that the magnitude of the electrostrictive interaction is sufficient to explain the observed volume contraction of the liquid.

ACKNOWLEDGMENTS

This research has been supported by the National Science Foundation under Grant No. DMR-83-20547.

[1]S. S. Kao and M. Cutler, Phys. Rev. B **37**, 10 581 (1988).
[2]J. A. Gardner and M. Cutler, Phys. Rev. B **20**, 529 (1979).
[3]H. P. Seyer, K. Tamura, H. Hoshino, H. Endo, and F. Hensel, Ber. Bunsenges. Phys. Chem. **90**, 587 (1986).
[4]H. Thurn and J. Ruska, J. Non-Cryst. Solids **22**, 331 (1976).
[5]K. Takimoto and J. Ruska, Phys. Chem. Liq. **12**, 141 (1982).
[6]S. Takeda, H. Okazaki, and S. Tamaki, J. Phys. Soc. Jpn. **54**, (1985).
[7]R. Bellisent and G. Tourand, J. Non-Cryst. Solids **35/36**, 1221 (1980).
[8]J. R. Magaña and J. S. Lannin, Phys. Rev. B **29**, 5663 (1984).
[9]H. Richter, J. Non-Cryst. Solids **8/10**, 388 (1972).
[10]B. Cabane and J. Friedel, J. Phys. **32**, 73 (1971).
[11]G. Tourand and M. Breuil, J. Phys. (Paris) **32**, 813 (1971).
[12]M. Cutler and H. Rasolondramanitra, *Localization and Metal-Insulator Transitions,* edited by H. Fritsch and D. Adler (Plenum, New York 1985), p. 199.
[13]M. Cutler, *Liquid Semiconductors* (Academic, New York, 1977).
[14]M. H. Cohen and J. Jortner, J. Phys. (Paris) Colloq. **35**, C4-435 (1974).
[15]Y. Tsuchiya and E. F. Seymour, J. Phys. C **15**, L687 (1982).
[16]R. J. Hodgkinson, Philos. Mag. **23**, 673 (1971).
[17]R. Fainschtein and J. C. Thompson, Phys. Rev. B **27**, 5967 (1983).
[18]L. A. Silva and M. Cutler, Rev. Sci. Instrum. **60**, 3078 (1989).
[19]See, for example, *Semiconductor Opto-Electronics,* T. S. Moss, G. J. Burrell, and B. Ellis (Wiley, New York, 1973).
[20]There are many papers on this topic in the literature, but no consensus has been reached for the mechanism behind this behavior. The following papers provide an introduction to the topic: H. Sumi and Y. Toyozawa, J. Phys. Soc. Jpn. **31**, (1971); J. D. Dow and D. Redfield, Phys. Rev. B **1**, (1970).
[21]J. Tauc, Prog. Semiconduct. **9**, 87 (1965).
[22]N. K. Hindley, J. Non-Cryst. Solids **5**, 17 (1970).
[23]J. D. Joannopoulos, M. Schlüter, and M. L. Cohen, Phys. Rev. B **11**, 2186 (1975).
[24]K. Maschke and P. Thomas, Phys. Status Solidi **41**, 743 (1970).
[25]J. Rabit and J. C. Perron, Phys. Status Solidi **65**, 255 (1974).
[26]F. G. Bell, and M. Cutler, Phys. Rev. B **34**, 5270 (1986).
[27]J. C. Perron, Doctoral thesis, University of Paris, 1969.
[28]M. Zanini and J. Tauc, Appl. Opt. **15**, 3149 (1976).
[29]T. E. Faber, *Introduction to the Theory of Liquid Metals* (Cambridge University Press, Cambridge, England, 1972).
[30]M. Cutler, S. S. Kao, and L. Silva, Phys. Rev. B **41**, 3339 (1990).
[31]J. E. Enderby and A. C. Barnes, Rep. Prog. Phys. **53**, 85 (1990).

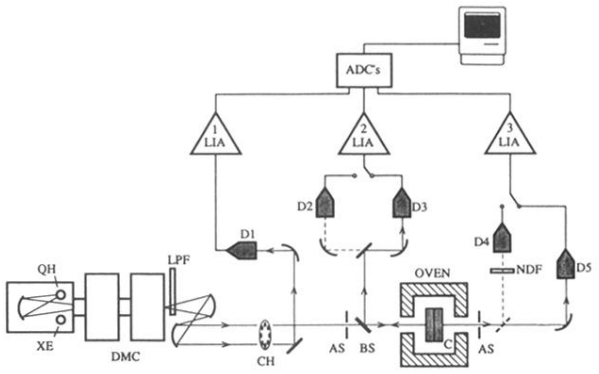

FIG. 1. Optical spectrometer: D1, pyroelectric detector; D2, PbS detector; D3, Si photodiode; D4, photomultiplier; D5, Si photodiode/PbS cell; QH, quartz-halogen lamp; XE, xenon arc lamp; LPF long-pass filter; DMC, double monochromator; LIA, lock-in amplifier; CH, chopper; AS, aperture stop; BS beam splitter; C, sample cell, NDF, neutral density filter.

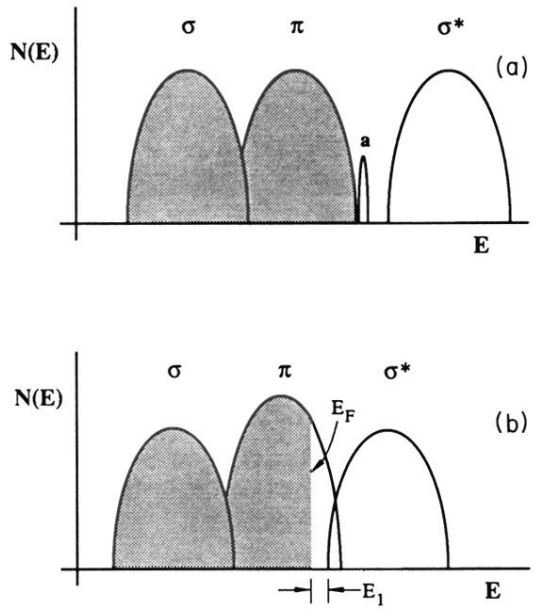

FIG. 13. Semiconductor-metal transition in Se-Te liquids as proposed by Cutler. (a) σ and σ^* bands are from intrachain bonding; lone-pair p orbitals from the π band. Broken bonds produce acceptor states a, and as the density of these defects increases an acceptor band shifts into the valence band (b). The Fermi level E_f falls at an energy E_1 below the conduction-band edge.